

Elastomeric diffraction gratings as photothermal detectors

John A. Rogers, Rebecca J. Jackman, Olivier J. A. Schueller, and George M. Whitesides

A photothermal detector consisting of a relief grating on the surface of an elastomer was fabricated and characterized. The detector has a sensitivity of the order of microwatts per square millimeter and has rise and fall times of the order of tens of seconds. Numerical and analytical modeling account for the behavior of the detector. © 1996 Optical Society of America

Key words: Thermal detector, diffraction, phase grating, elastomer.

1. Introduction

In this paper we describe the fabrication and performance of a thermal detector based on an elastomeric diffraction grating. The device consists of a binary-phase surface-relief grating on a millimeter-thick section of polydimethylsiloxane (PDMS). The operating principle of this detector is as follows: Thermal expansion induced by absorption of light causes a shift in the angular positions of light beams diffracted from the grating. This shift can be related quantitatively to the intensity of the absorbed light. PDMS elastomers are well suited to this application: They have large coefficients of thermal expansion [3×10^{-4} cm/(cm °C)]; they can be easily molded into surface relief gratings¹; they are transparent in the ultraviolet-visible range (300–800 nm); and their sensitivity can be tailored to the optical wavelength of the heating light by doping with dyes.

A class of strain gauge based on an operating principle similar to the detector described here has been used extensively for the measurement of surface strain fields.^{2–7} These gauges consist of diffraction gratings deposited on a sample. As the sample responds to body forces, the pattern of diffraction changes. These changes are used to determine the strain near the location of the diffraction grating. Although this class of diffraction-based device is valu-

able in applied mechanics, we are not aware of related applications in optical detection.

Conventional thermally based optical detectors measure changes in resistivity (bolometer), in internal dipole moment (pyroelectric detector), in potential across the junction of two dissimilar metals (thermopile) as a function of temperature, or in the position of a beam of light reflecting from a deformable mirror (Golay detector).^{8–11} Microthermopiles, fabricated by techniques compatible with silicon processing, have been used as multipurpose sensors to monitor infrared radiation, ambient pressure, and gas flow.^{12,13} Although the sensitivity of the elastomeric grating detector described in this paper is lower than that of many of these conventional detectors, it is a simple, low-cost device. We believe that slight modifications to the design of the detector will yield a significant increase in its sensitivity.

This paper begins with a description of the fabrication of the device. A theoretical description of the behavior of the response of the detector to heating induced by absorption of light adequately models the experimental results. Analytical results describe the angular shifts of the diffracted beams and account for the rise time of the detector. Finite-element modeling (FEM) elucidates nonidealities in the behavior of the detector. Experimental results establish the rise time and the sensitivity of the detector. These results compare favorably with theoretical description.

2. Experiment

The elastomeric gratings were fabricated by casting PDMS prepolymer (Dow Corning Sylgard 184) onto a master with 2- μ m parallel lines of photoresist (~ 1 μ m thick) spaced 2 μ m apart on a silicon wafer (Fig.

The authors are with the Department of Chemistry, Harvard University, Cambridge, Massachusetts 02138.

Received 12 February 1996; revised manuscript received 8 April 1996.

0003-6935/96/346641-07\$10.00/0

© 1996 Optical Society of America

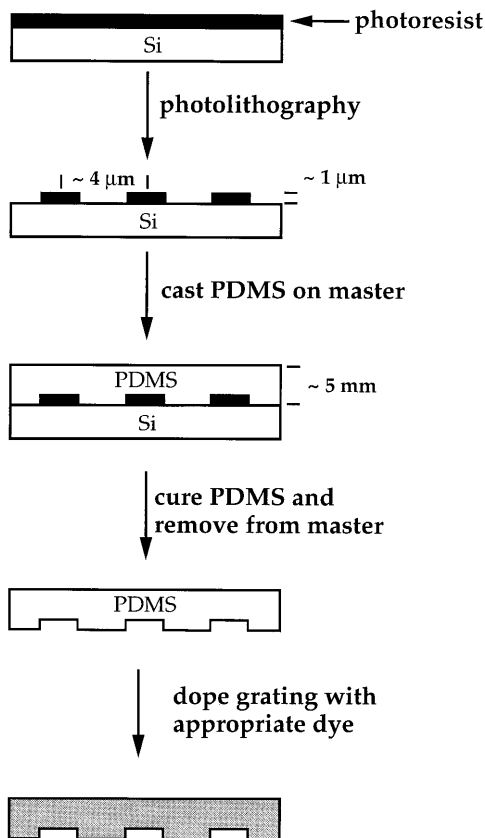


Fig. 1. Fabrication of elastomeric surface-relief phase grating. The elastomeric grating was fabricated by casting of PDMS prepolymer onto a master produced by photolithography. After curing, the elastomeric grating was removed from the master and doped with Sudan Red.

1). After curing, the PDMS was removed from the master, yielding a free-standing elastomeric phase grating. To induce optical absorption near 500 nm, the grating was doped with Sudan Red 7B ($\lambda_{\max} \sim 533$ nm) by placing the grating into an ethanol:hexane (3:2) solution saturated with Sudan Red (Aldrich) for ~ 30 min. After being rinsed thoroughly with ethanol, the grating was heated overnight to drive off the remaining solvent. The absorption length of the grating was 1700 m^{-1} .

Characterization of the gratings as photothermal detectors was performed with the experimental setup illustrated schematically in Fig. 2. Light from an Ar^+ laser (514 nm), the heating laser, was directed to the grating. Light from a He-Ne laser (633 nm), the probing laser, was overlapped with the heating beam on the elastomeric grating sample. To minimize problems associated with thermal lensing (described in Subsection 3.A.2) the diameter of the probing beam (~ 1 mm) was made small compared with that of the heating beam (~ 1 cm). The probing beam was well centered in the heated region of the sample.

Expansion induced by the heating beam was detected by measurement of the angular deflection of the diffracted probing beams arising from passage through the grating. The angular deflection was

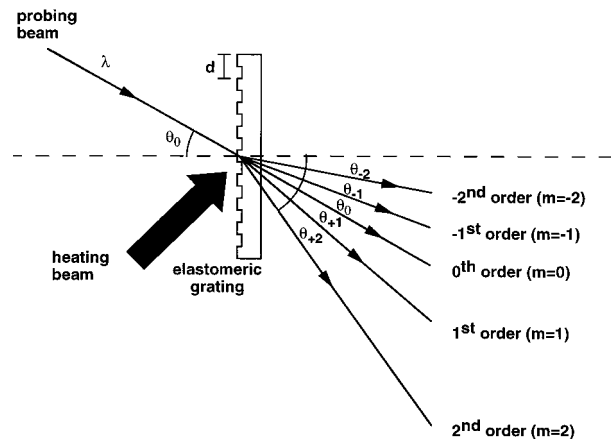


Fig. 2. Schematic illustration of characterization of the photothermal detector. Lateral thermal expansion induced by absorption of the heating light changes the wavelength of the grating. The change in wavelength is monitored by deflection of diffracted orders of a probing laser beam. Higher-order diffracted beams ($|m| > 2$) have been omitted from the figure for clarity.

measured as a function of the intensity of the heating beam. For linear deflections larger than 1 mm, distances were measured with a ruler. Smaller deflections were measured with a CCD camera. The response time was determined by measurement of the angular deflection of a diffracted beam during the heating process by use of a CCD camera.

3. Results and Discussion

A. Theory

Simple theoretical arguments explain the experimental behavior of the device. First an expression for the angular shift of diffracted beams as a function of temperature, the coefficient of thermal expansion, the wavelength of the grating, and the probing angle of incidence is derived. This expression accurately accounts for experimental observations and indicates several ways to optimize the sensitivity of the device. FEM of the optically induced thermal expansion is described. The FEM results show that a thermal lens, or bump, forms on the surface of the device when it is heated. This thermal lens must be considered when the performance of the device is modeled. Finally, analytical results for heat flow in a semiinfinite body are presented. These results illustrate how parameters governing the flow of heat determine the sensitivity and time response of the device.

1. Thermally Induced Angular Shift of Diffracted Beams.

For a given expansion, the highest-order diffracted beams generated by probing at large angles of incidence undergo the largest angular deflections.

Light diffracted from a grating appears in angular locations determined by

$$\sin \theta - \sin \theta_0 = \frac{m\lambda}{d}, \quad (1)$$

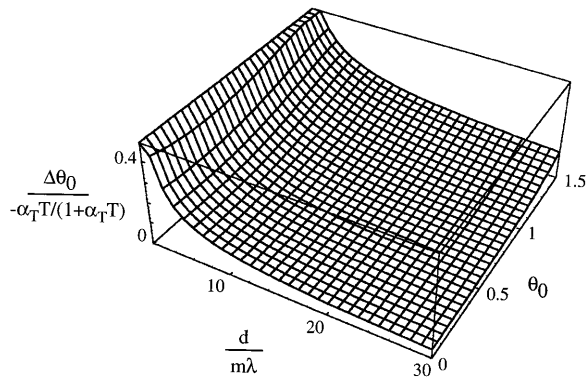


Fig. 3. Normalized angular deflection, $\Delta\theta_m/[-\alpha_T T/(1 + \alpha_T T)]$, plotted as a function of $d/m\lambda$ and θ_0 , where m is the diffracted order, d is the wavelength of the grating, λ is the optical wavelength, and θ_0 is angle of incidence of the probing beam. For a given expansion, the largest changes in diffraction angle are produced when $d/m\lambda$ is small and the incidence angle is large.

where θ_m is the angle of diffraction for the m th-order beam, θ_0 is angle of incidence of the probing beam, λ is the wavelength of the probing light, and d is the wavelength of the diffraction grating. Figure 2 illustrates the quantities appearing in Eq. (1).

Thermal expansion induces a change in the wavelength of the grating. This change is proportional to the change in temperature and the coefficient of thermal expansion and is given by

$$d_T = d + \Delta d = d(1 + \alpha_T T), \quad (2)$$

where d_T is the wavelength of the grating after the temperature increases by T , and α_T is the coefficient of thermal expansion.

Using Eqs. (1) and (2), it is straightforward to show that, when the expansion is small ($\alpha_T T \ll 1$), the change in diffraction angle for the m th-order diffracted beam $\Delta\theta_m$ is given by

$$\Delta\theta_m = \frac{-\alpha_T T / (1 + \alpha_T T)}{\{(d^2/m^2\lambda^2) - [1 + (d/m\lambda)\sin\theta_0]^2\}^{1/2}}. \quad (3)$$

Figure 3 shows $\Delta\theta_m/[-\alpha_T T/(1 + \alpha_T T)]$ as a function of $d/m\lambda$ and the probing angle θ_0 . This figure shows that the sensitivity of the device is maximized when $d/m\lambda$ is small and θ_0 is large.

2. FEM of the Photothermal Expansion of the Device.

The heating laser generates a bump on the surface of the device that must be taken into account when the performance of the device is determined.

In Subsection 3.A.1 a simple expression was used to relate the magnitude of the mechanical strain ($\Delta d/d$) to the temperature rise. In a real experiment, the heating laser has a finite spot size that induces nonuniform strain on the surface of the device. In particular, the localized heating induced by this laser generates a bump on the surface of the device. FEM confirms this expectation.

Two-dimensional, steady-state, thermoelastic

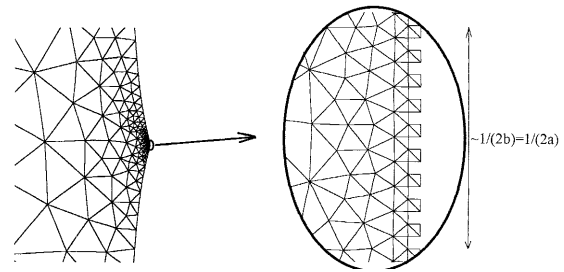


Fig. 4. FEM analysis of the heating of an elastomeric grating structure by a laser beam. The steady-state results show the formation of a bump whose width is of the order of the laser-beam spot size. At the center of this bump, the expansion of the material is approximately spatially homogeneous (right frame of the figure).

FEM computations were performed in the plane-strain limit. The surface of the device was assumed to be large compared with the extent of the heating, and the surface was assumed to be free of stress. The flow of heat from the surface of the device to the surroundings was assumed to be Newtonian. The deformed finite-element mesh resulting from these computations is illustrated in Fig. 4. The lateral dimensions of the bump illustrated in this figure are comparable with the size of the area illuminated by the heating laser. The height of the bump ranges from nanometers to micrometers for the experiments described here.

For characterizing and understanding the behavior of the device, this bump, which has the optical properties of a lens, must be taken into account. The lensing effects associated with the bump are minimized when the spot size of the probing beam is small relative to the heating beam and the probing beam is centered in the heating beam. The effects are minimized because the lateral displacements of the grating near the center of the heating beam are only weak functions of the distance from the center (Fig. 4). If the size of the probing beam is comparable with that of the heating beam and the probing and heating beams are not perfectly overlapped, then the formation of the bump will cause deflections of the transmitted probing light. These deflections can either add to or subtract from the deflections induced by a change in the wavelength of the grating.

3. Time Dependence of the Temperature of the Surface of the Device During Heating.

The sensitivity and response time of the device are determined by the coefficient of thermal expansion and by parameters governing the flow of heat in the device.

In addition to the steady-state finite-element computations, analytical expressions were derived for the time dependence of the temperature of the device during and after heating. The temperature of the device in the region of the grating determines the change in the wavelength of the grating. To solve for the temporal evolution of this quantity, the thermal response to impulsive heating is evaluated and

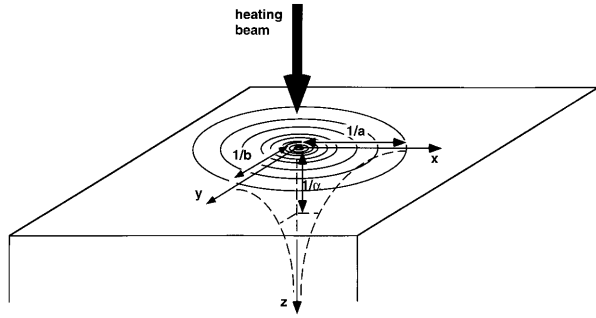


Fig. 5. Definition of the coordinate system and geometrical quantities used in the computation of the dynamics of heat flow. The contours represent equal intensities of the heating beam. The dashed curves represent the depth of penetration of the heating beam, where $1/\alpha$ is the absorption length.

then convolved with the temporal dependence of the heating light. The relevant equations follow. The coordinate system is illustrated in Fig. 5.

$$\frac{\partial T}{\partial t} = D\nabla^2 T + \frac{I_{\text{abs}}\alpha}{\rho C} \exp(-\alpha z) \times \exp(-b^2 y^2) \exp(-a^2 x^2) \delta(t), \quad (4)$$

$$T(t = 0) = 0, \quad (5)$$

$$T(z \rightarrow \infty) = 0, \quad (6)$$

$$\left. \frac{\partial T}{\partial z} \right|_{z=0} = \frac{R}{D} T|_{z=0}. \quad (7)$$

The change in temperature is T (Kelvin), $\delta(t)$ is the Dirac delta function centered at $t = 0$, D is the isotropic thermal diffusivity (square meters per second), α is the absorption length (per meter), $1/b$ is the heating spot size in the y direction (meters), $1/a$ is the spot size in the x direction (meters), and R defines the rate of Newtonian heat flow from the device to the surroundings (meters per second). The intensity of light absorbed by the device is I_{abs} (joules times inverse seconds times inverse square meters), ρ is the density (kilograms times cubic meters), and C is the heat capacity per unit mass (joules times inverse kelvins times inverse kilograms). The solution to these equations can be written as

$$T(x, y, z, t) = \frac{I_{\text{abs}}\alpha}{\rho C} \exp(-\alpha z) X(x, t) Y(y, t) F(z, t), \quad (8)$$

where

$$Y(y, t) = \frac{\exp[-y^2 b^2 / (1 + 4Dt b^2)]}{(1 + 4Dt b^2)^{1/2}}, \quad (9)$$

$$X(x, t) = \frac{\exp[-x^2 a^2 / (1 + 4Dt a^2)]}{(1 + 4Dt a^2)^{1/2}}, \quad (10)$$

and $F(z, t)$ solves the following equations:

$$\frac{\partial F}{\partial t} = D\alpha^2 F - 2D\alpha \frac{\partial F}{\partial z} + D \frac{\partial^2 F}{\partial z^2}, \quad (11)$$

$$F(t = 0) = 1, \quad (12)$$

$$\left. \frac{\partial F}{\partial z} \right|_{z=0} = cF|_{z=0}, \quad (13)$$

where $c = \alpha + R/D$. $X(x, t)$ and $Y(y, t)$ describe thermal diffusion in the x and the y directions, respectively, and $\exp(-\alpha z)F(z, t)$ describes the flow of heat in the out-of-plane direction.

Using transform techniques, it can be shown that F is given by

$$F(z, t) = \frac{c \exp(2\alpha z) \exp(D\alpha^2 t)}{2(\alpha - R/D)} \operatorname{erfc} \left[\left(\frac{z}{2\sqrt{Dt}} + \alpha\sqrt{Dt} \right) \right] + \exp(D\alpha^2 t) - \frac{\exp(D\alpha^2 t)}{2} \times \operatorname{erfc} \left[\left(\frac{z}{2\sqrt{Dt}} - \alpha\sqrt{Dt} \right) \right] + \frac{(R/D) \exp(cz) \exp(R^2 t/D)}{R/D - \alpha} \times \operatorname{erfc} \left[\left(\frac{z}{2\sqrt{Dt}} + R\sqrt{t/D} \right) \right], \quad (14)$$

where erfc is the complementary error function.

From the impulsive solution given in Eqs. (8)–(10) and (14), the temperature during heating by light that has temporal dependence defined by $f(t)$ is T_{ni} , the nonimpulsive temperature response:

$$T_{\text{ni}}(x, y, z, t) = \int_{-\infty}^t T(x, y, z, t - t') f(t') dt'. \quad (15)$$

In the limiting case that $b = a$ and $R = 0$, our result is consistent with that of Betchel.¹⁴ For the experiments described here the heating laser pulse has the form

$$f(t) = \begin{cases} 0 & t \leq 0 \\ 1 & 0 < t \leq \tau \\ 0 & t > \tau \end{cases} \quad (16)$$

The temporal duration of the heating is τ . Using this form to integrate Eq. (15) numerically yields the temperature of the grating as a function of time during and after the heating. Figure 6 shows the temporal evolution of the surface temperature of the device. When the flow of heat into the depth of the device dominates the behavior of the temperature at the surface (R is small, and $1/b$ and $1/a$ are large), the temperature increases without bound, with the increase having approximately the form¹⁴ $t^{1/2}$. In a real system the temperature of the device reaches a steady state when the rate at which heat is generated

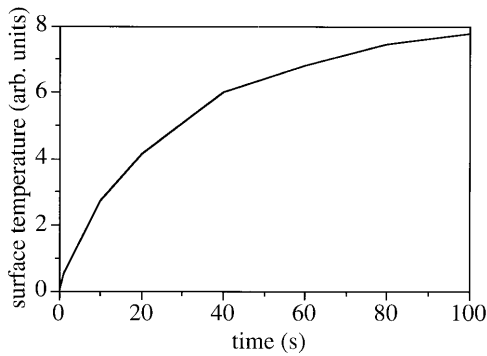


Fig. 6. Surface temperature as a function of time for a semi-infinite body heated by a continuous-wave laser. The parameters for the simulation shown here were as follows: $\alpha = 1000.0 \text{ m}^{-1}$, $D = 5.0 \times 10^{-7} \text{ m}^2/\text{s}$, $R = 1.0 \times 10^{-6} \text{ m/s}$, $b^{-1} = 0.5 \text{ cm}$, $a^{-1} = 0.5 \text{ cm}$. The values of α , b^{-1} , and a^{-1} were measured. R and D are typical for the sort of system investigated here and were taken from the literature.^{15,16}

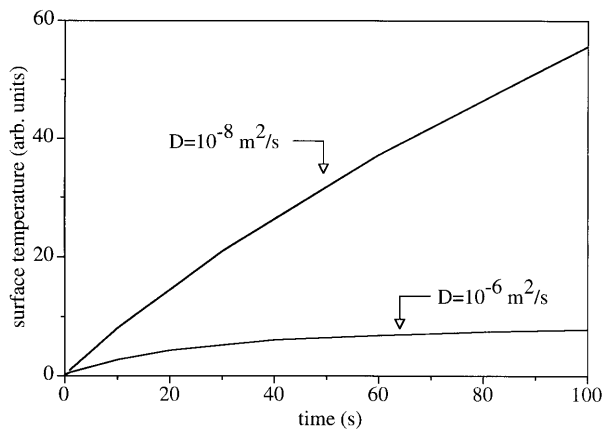


Fig. 7. Surface temperature as a function of time for two semi-infinite bodies heated by a continuous-wave laser. Only the thermal diffusivity of the materials is different. In the material with lower diffusivity, the temperature rise is slower but, in a given amount of time, reaches a higher value than the temperature in the material with higher thermal diffusivity. As a result, if all other material properties remain the same, increasing the thermal diffusivity of the detector will cause the rise time and the sensitivity to decrease.

by the heating laser is equal to the rate at which heat is removed by convective and other losses.

The equations in this section illustrate how the sensitivity and rise time of the device are affected by variables that determine the dynamics of the flow of heat. In particular, these equations show that increases in sensitivity can be obtained when the rate of heat flow out of the device or away from the region of the device near the surface is restricted or slowed. To accomplish the reduction in the flow of heat, the device could be sealed in an evacuated cell or could be constructed of a material with a low thermal diffusivity. The equations also show that to decrease the rise time of the device, the time required to establish equilibrium between the device and the surroundings should be decreased. This equilibrium is estab-

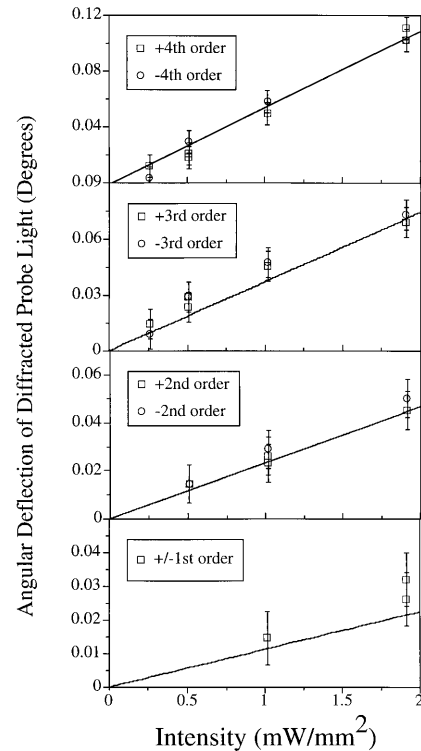


Fig. 8. Data (symbols) showing angular deflections of the plus or minus first-, second-, third-, and fourth-order diffracted beams as a function of the intensity of the heating light. Green light (514 nm) was used to heat, and red light (633 nm) was used to probe. The detector consisted of a PDMS grating doped with Sudan Red. The solid line in the top panel, illustrating the angular deflection of the plus or minus fourth-order, represents the best linear fit to the data. The solid lines in the other panels were generated with the best-fit slope for the fourth-order data and Eq. (3) and involve no additional fitting parameters.

lished when the rate of flow of heat into the device and away from the region of the device near the grating are equal. To decrease the time required to reach equilibrium, the device could be surrounded by material that would efficiently draw heat from the device. Also, the device could be fabricated from material with a high thermal diffusivity in order to increase the rate of flow of heat to the bulk of the device. In this way, when the flow of heat out of the device can be neglected, the time required for the time rate of change of the surface temperature to fall below a given value could be reduced. Some of these ideas are illustrated in Fig. 7; this figure suggests the time dependence of the surface temperature of two devices made from materials with different thermal diffusivities when the flow of heat out of the device and into the surroundings is negligible. All other parameters describing the devices are unchanged. Figure 7 shows that the temporal derivative of the surface temperature of the material with high thermal diffusivity approaches a small value more quickly than the corresponding quantity for the material with low thermal diffusivity. Figure 7 also shows that, at any given time after $t = 0$, the surface temperature of the material with low thermal diffusivity is higher than

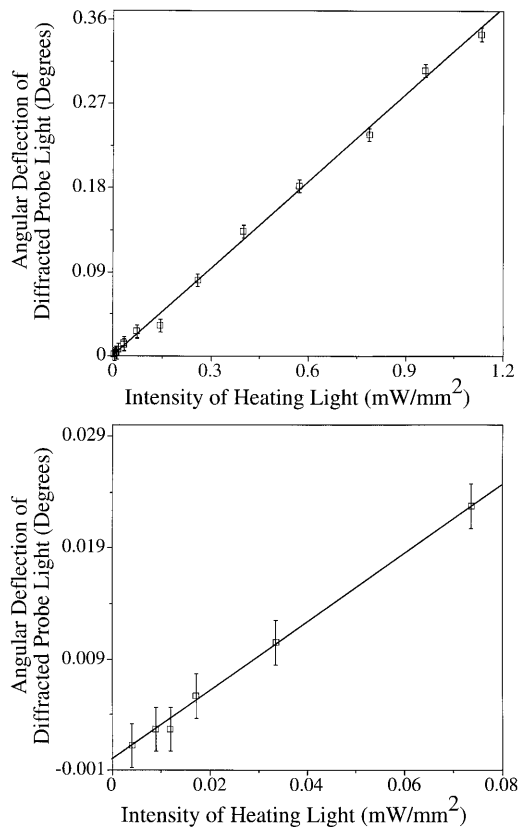


Fig. 9. Data showing angular deflections of the ninth-order beam as a function of the intensity of the heating light. The probing angle of incidence was 42° . The data illustrate sensitivity to microwatts per square millimeter.

the surface temperature of the material with high thermal diffusivity. In other words, the sensitivity of the device made from a high-diffusivity material is lower than a similar device constructed from material having a lower thermal diffusivity.

B. Experiment

Figure 8 plots the angular deflections in the first-, second-, third-, and fourth-order spots of the probing beam (normal incidence) induced by heating light as a function of the intensity of the heating beam. Deflections of each of the diffracted beams are related to one another according to Eq. (3). To evaluate the sensitivity of our detector, we performed calibration measurements using the one of the highest-order observable diffracted beams (in our case, the ninth-order spot) at a large (42°) probing angle. Figure 9 illustrates the results. As with the first four diffracted beams, the ninth-order beam exhibited an angular deflection related linearly to the intensity of the heating light. The sensitivity limit of this detector is of the order of microwatts per square millimeter. For intensities in this range the change in grating wavelength is of the order of 1 part in 10^5 , which corresponds to a change in periodicity of 0.2 \AA for a grating with a wavelength of 4 \mu m . Using Eq. (3), the measured angular shifts and the linear thermal expansion coefficient for PDMS, we calculated

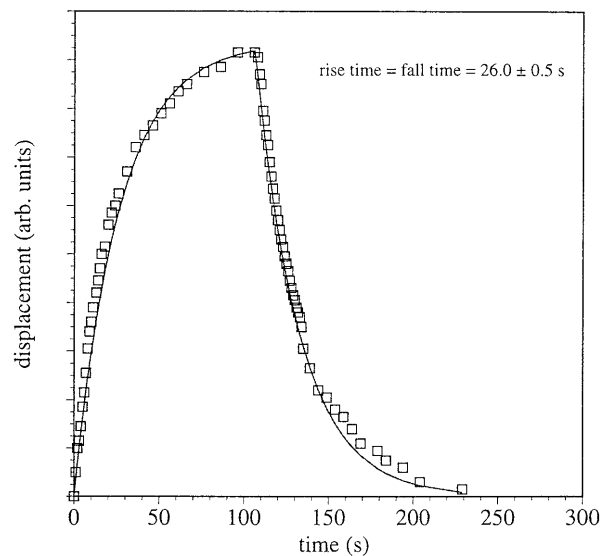


Fig. 10. Data showing the angular deflection of the fourth-order beam as a function of time after the detector is exposed to heating light. The lines represent empirical fits of the data to a single exponential rise and fall. The rise and fall times determined from these fits were $\sim 25 \text{ s}$.

that the heating laser induced temperature changes of between 0.01 and 10 K near the surface of the grating.

The rise and fall times of the device were determined by measuring the angular deflection of the fourth-order diffracted beam as a function of time during the heating process; a CCD camera was used for the measurement. Figure 10 shows the linear displacement of the beam as a function of time. Fitting the experimental data empirically with an exponential curve gave rise and fall times of $\sim 25 \text{ s}$. The experimental rise time is comparable with the analytical calculations for time-dependent heat flow in a semi-infinite body described in Subsection 3.A.3 and illustrated in Fig. 6. Because of uncertainties in physical properties of our detector and inadequacies in the theoretical model, detailed quantitative comparison between experimentally measured and theoretically predicted rise times was not attempted.

4. Conclusions

A frequency-sensitive photothermal detector was fabricated with doped PDMS elastomers. Thermal expansion induced by absorption of heating light by dye molecules resulted in a shift in the angular positions of light beams diffracted from the grating. This detector has a sensitivity of the order of microwatts per square millimeter and a rise and fall time of 25 s. As mentioned in the introduction, there are means for increasing the sensitivity of the device. These improvements include thermally isolating the grating, exploiting the redundancy in the data provided by multiple-diffracted beams, or using different surface-relief structures for generating the diffracted light.

This research was supported in part by the National Science Foundation (NSF, PHY-9312572). It also used MRSEC Shared Facilities supported by the NSF under award DMR-9400396. We extend our thanks to Keith Nelson of M.I.T. for the use of lasers and laboratory. J. A. Rogers gratefully acknowledges funding from the Harvard University Society of Fellows, and R. J. Jackman gratefully acknowledges a scholarship from the Natural Sciences and Engineering Research Council of Canada.

References

1. J. L. Wilbur, R. J. Jackman, G. M. Whitesides, E. Chang, L. Lee, and M. Prentiss, "Elastomeric Optics," *Chem. Mater.* **8**, 1380–1385 (1996).
2. S. B. Brown, U.S. Patent 4,939,368 (3 July 1990).
3. P. M. Boone, "A method for directly determining surface strain fields using diffraction gratings," *Exp. Mech.* **11**, 481–489 (1971).
4. T. Yamamoto, M. Kawase, and H. Sato, "Direct measurement of piezoelectric strain using a diffraction grating," *J. Am. Ceram. Soc.* **70**, 557–561 (1987).
5. C. A. Sciammarella and H. Nyuko, "Two new optical techniques to measure strain," *Exp. Mech.* **14**, 311–316 (1974).
6. R. Ruby, D. Baldwin, and M. Karnezos, "The use of diffraction techniques for the study of in-plan distortions of x-ray masks," *J. Vac. Sci. Tech.* **B5**, 272–277 (1987).
7. A. Olivares-Perez, L. R. Berriel-Valdos, J. L. Juarez-Perez, and F. Mendoza Santoyo, "Dynamic holographic gratings with photoresist," *Appl. Opt.* **34**, 5577–5581 (1995).
8. R. S. Keyes, *Optical and Infrared Detectors*, Vol. 19 of Topics in Applied Physics (Springer-Verlag, Berlin, 1977).
9. L. Levi, *Applied Optics* (Wiley, New York, 1980), Vol. 2, Chap. 16, pp. 582–600.
10. R. H. Kingston, *Detection of Optical and Infrared Radiation* (Springer-Verlag, Berlin, 1978), Chap. 7, pp. 83–100.
11. M. J. E. Golay, "A pneumatic infra-red detector," *Rev. Sci. Instrum.* **18**, 357–362 (1947).
12. M. A. Gajda and H. Ahmed, "Applications of thermal silicon sensors on membranes," *Sensors Actuators A (Phys.)* **A49**, 1–9 (1995).
13. T. A. S. Srinivas and H. Ahmed, "Multi-purpose sensor based on free-standing microthermopiles," in *Smart Structures and Materials 1994: Smart Structures and Intelligent Systems*, N. W. Hagood, ed., Proc. SPIE **2448**, 2–8 (1995).
14. J. H. Betchel, "Heating of solid targets with laser pulses," *J. Appl. Phys.* **46**, 1585–1593 (1975).
15. H. S. Carslaw and J. C. Jaeger, *Conduction of Heat in Solids*, 2nd ed. (Oxford U. Press, London, 1959), 18–23.
16. J. Brandup and E. H. Immergut, *Polymer Handbook*, 3rd ed. (Wiley-Interscience, New York, 1989), pp. V7–V13.